Continuum micromagnetic modeling of antiferromagnetically exchange-coupled multilayers

R. Pellicelli, M. Solzi, C. Pernechele, and M. Ghidini
Dipartimento di Fisica e CNISM, Università di Parma, Via G. P. Usberti 7/A, I-43100 Parma, Italy
(Received 22 October 2010; revised manuscript received 16 December 2010; published 25 February 2011)

The micromagnetic continuum theory has been applied to perfect soft/hard multilayers characterized by antiferromagnetic interface coupling. The soft and hard phases have uniaxial anisotropy with a common direction, along which the external field is applied. The model assumes a nonuniform rotation of the magnetization, and it also considers an interface coupling that is reduced with respect to the strong-limit case. It is found that the deviation of the magnetization from the saturated antiparallel state can occur at two distinct nucleation fields, which mainly involve only one of the two phases. Moreover, in the case of a reduced interface coupling, the saturated parallel state becomes accessible and thus the nucleation from this state is taken into account. The critical equations have been deduced, allowing us to identify the conditions for which the nucleation regime changes from reversible to irreversible as a function of the intrinsic and extrinsic parameters. The results of the model, applied to a typical soft/hard system with planar anisotropy, have been summarized in suitable phase diagrams, as a function of the layer thicknesses and of the strength of the interface coupling. The analysis, supported by additional static and dynamic micromagnetic simulations, shows the occurrence of a rich variety of magnetization curves. As a secondary result we have found that, in the parallel nucleation process, the influence of the interface coupling extends inside the two phases to distances appreciably larger than the corresponding Bloch wall widths.

DOI: 10.1103/PhysRevB.83.054434 PACS number(s): 75.70.Cn, 75.60.Jk, 75.60.Ej

I. INTRODUCTION

Exchange-coupled magnetic systems,[1–5] also called exchange-spring magnets,[6] have long been known[7] for specific properties that make them attractive in application areas such as permanent magnets[6] and magnetic recording.[1,8] A particular variant of these systems, in which the interface exchange coupling between two ferromagnetic phases is antiferromagnetic, has recently drawn a great deal of attention for applications in the field of spintronics, magnetic recording, and sensing devices.[9–18] The rich variety of magnetic behaviors that arises from the antiferromagnetic character of the interface coupling[19–22] needs a theoretical analysis to ensure a complete comprehension of this complex phenomenology.

The micromagnetic continuum theory[23] has been applied here to perfect soft/hard bilayers and multilayers, characterized by uniaxial planar anisotropy and antiferromagnetic exchange coupling at the interface between the two ferromagnetic phases. The soft and hard phases have identical anisotropy axis direction, along which the external field is applied. Both cases of strong and reduced interface coupling[24,25] are considered. The continuum approach[26] allows the analytical deduction of equations that can effectively support the results obtained by discrete models,[27–29] with particular reference to one-dimensional systems. Moreover, the developed mathematical treatment, which considers the nonuniform rotation of magnetization in the plane of the bilayers, does not impose any limits to the allowed layer thicknesses or interface coupling strength, as is implicitly assumed in the case of coherent rotation.[9] A more general aspect of the performed analysis is that the equations obtained are in principle valid without any *a priori* restriction on the possible values of all the intrinsic and extrinsic parameters, in contrast to other works in which such restrictions are adopted.[30–32]

The magnetization process is studied starting from the antiparallel state, in which the soft and hard phases are saturated along opposite directions. Similarly to the case of ferromagnetic interface coupling treated in Ref. 33, the equations for the nucleation fields, at which the magnetization begins to deviate from the antiparallel state, are derived. Moreover, the critical equations are deduced that determine when the nucleation processes occur in a reversible or irreversible way. In the case of a reduced interface coupling, the parallel state, in which the soft and hard phases are saturated along the same direction, also becomes accessible. Therefore, the corresponding nucleation field equation and critical equation are calculated. All the possible behaviors of a soft/hard system can be summarized in general phase diagrams as a function of the desired intrinsic and extrinsic parameters. The analytical results obtained are in principle valid for both planar and perpendicular anisotropy,[34–37] even though, in the perpendicular case, the antiparallel and parallel states are allowed only for restricted ranges of the parameters. However, the perpendicular configuration is not taken into account in this work. The developed model is in particular applied to a typical soft/hard system in order to obtain the phase diagrams as a function of the layer thicknesses and of the interface coupling strength. We note that in practical realizations of these systems, the interface coupling strength can be typically tuned by adjusting the thickness of a nonmagnetic spacer layer.[38–40] In addition to the phase diagrams, complete hysteresis loops are calculated by means of both static and dynamic simulations.

The paper is organized as follows. The general theoretical treatment is presented in Sec. II. The model is then applied in Sec. III to bilayers in which the hard layer has an ideal infinite anisotropy, distinguishing between the antiparallel (Sec. III A) and the parallel (Sec. III B) nucleation processes. The general case is treated in Sec. IV, where the antiparallel nucleation process is analyzed in Sec. IV A and applied to the case of strong interface coupling in Sec. IV B. The

reduced interface coupling is then studied in Sec. IV C, which includes in particular the description of the parallel nucleation process.

II. MODELING OF THE MAGNETIZATION PROCESS

A. Micromagnetic continuum theory

In the framework of the micromagnetic continuum theory, the magnetization vector inside a ferromagnetic phase is a continuous function of the space-time coordinates.[23] The dynamics of the magnetization is determined by the torque acting on the magnetic moment of each volume element dV. This torque is due to the effective field H_{eff}, which is the negative functional derivative of the total magnetic Gibb's free energy.[41] The effective field coincides here with the sum of the exchange, anisotropy, and demagnetizing fields, as well as of the external magnetic field H. Concerning in particular the exchange interaction between two adjacent volume elements characterized by distance dr, interface area dS, and magnetization directions $\vec{m}$ and $\vec{m}' = \vec{m} + (d\vec{m}/dr)dr$, respectively, the corresponding exchange energy is $dw_{\text{ex}} = 2J(1 - \vec{m}\cdot\vec{m}')dS = J(\vec{m}' - \vec{m})^2 dS = Jdr(d\vec{m}/dr)^2 dV$, where J denotes the strength of the interaction. Accordingly, one has to assume a strong exchange coupling inside the phase, which is equivalent to the condition $J \to \infty$ keeping $A = Jdr$ finite, in order to allow a non-negligible exchange energy density with respect to the other energy density terms. As a consequence, the torque $d\vec{c}_{\text{ex}} = -\vec{m} \times (\partial dw_{\text{ex}}/\partial\vec{m})dS = \vec{m} \times 2J(\vec{m}' - \vec{m})dS = \vec{m} \times 2J(d\vec{m}/dr)dV$ between the two volume elements turns out to be infinite with respect to the other torque terms. However, the resultant exchange torque $d\vec{C}_{\text{ex}} = \vec{m} \times 2A\nabla^2\vec{m}dV$ applied to $\vec{m}$ inside the ferromagnetic phase by all the adjacent volume elements is finite. On the contrary, such compensation is not present on a free surface (interface between ferromagnetic and nonmagnetic phases) along its normal direction n, since the infinite torque due to the adjacent internal volume element is not compensated by an external one. Therefore in this case the magnetization is forced to be oriented so that $d\vec{m}/dn = 0$. At the interface between two ferromagnetic phases Φ_1 and Φ_2, it is in general assumed that the strength J_{12} of the exchange interaction can also be finite ($|J_{12}| \leqslant \infty$), as a consequence of a possible reduced interface coupling.[24] When $|J_{12}| < \infty$, the infinite torques due to the strong coupling inside the two phases are compensated at the interface by a discontinuity in the $\vec{m}$ direction, so that the angle between the directions $\vec{m}_1$ and $\vec{m}_2$ at the two sides of the interface is finite. Therefore, the following conditions have to be fulfilled:

$$\begin{aligned} \frac{A_1}{J_{12}}\frac{d\vec{m}_1}{dn_1} &= (\vec{m}_2 - \vec{m}_2\cdot\vec{m}_1\vec{m}_1), \\ \frac{A_2}{J_{12}}\frac{d\vec{m}_2}{dn_2} &= (\vec{m}_1 - \vec{m}_1\cdot\vec{m}_2\vec{m}_2), \end{aligned} \tag{1}$$

where n_1 and $n_2 = -n_1$ are the outward-pointing normal directions in the two phases at the interface. From Eq. (1) one can deduce that in the case of strong interface coupling ($J_{12} \to \pm\infty$), the magnetization directions at the interface tend to be parallel ($\vec{m}_2 \to \vec{m}_1$) or antiparallel ($\vec{m}_2 \to -\vec{m}_1$). In the present work we assume that the sign of the interface exchange coupling is negative ($J_{12} < 0$), corresponding to an antiferromagnetic interface coupling between the ferromagnetic phases. Accordingly, the interface exchange torques $d\vec{c}_{\text{ex1}} = \vec{m}_1 \times 2J_{12}(\vec{m}_2 - \vec{m}_1)dS$ and $d\vec{c}_{\text{ex2}} = \vec{m}_2 \times 2J_{12}(\vec{m}_1 - \vec{m}_2)dS$ favor an antiparallel alignment of the magnetization directions at the interface.

B. Theoretical model

Let us consider an infinite soft/hard bilayer lying parallel to the yz plane [see Fig. 1(a)], characterized by magnetocrystalline anisotropy constants K_i, exchange stiffness constants A_i, saturation magnetizations M_i, and layer thicknesses t_i, where $i = 1,2$ for the bottom soft and top hard layers, respectively. We assume that, due to the perfect uniformity of the external field and of the physical properties in the planes of the system, the magnetization process can be described by means of a one-dimensional model, in which the magnetization depends only on the perpendicular coordinate x, and so its direction is expressed in general by the azimuthal angle $\vartheta(x)$ and by the polar angle $\varphi(x)$. We take into account here the case of planar anisotropy, characterized by anisotropy axes parallel to the z axis, with the external field H applied along the easy direction.

The equilibrium states of the bilayer, which are characterized by the unique angle $\vartheta(x)$,[7,42] can be deduced by

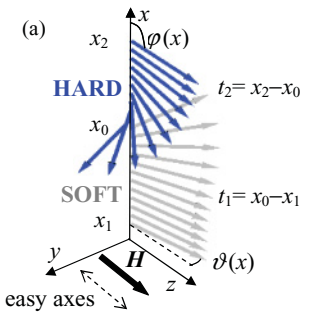

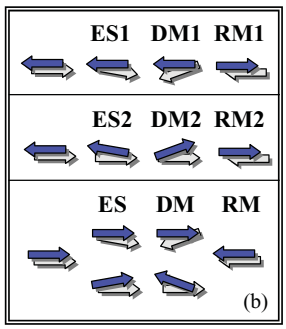

FIG. 1. (Color online) (a) Basic scheme for the one-dimensional micromagnetic model of a soft/hard exchange-coupled bilayer. The reported magnetic configuration corresponds to point P of Fig. 5(a). (b) Schematic representation of the magnetic configurations straight after nucleation, for all the possible nucleation regimes (the hard layer is at the top of each configuration and the initial state is on the left). In the bottom box, the two typical configurations are shown for the ES and DM cases. The labels ES1, DM1, RM1, ES2, DM2, RM2, ES, DM, and RM, are defined in the text.

analytically solving the micromagnetic equilibrium equation $\vec{m} \times \vec{H}_{\text{eff}} = 0$ with the boundary conditions introduced in Sec. II A. The mathematical procedure for solving this equation in the case of perpendicular anisotropy (anisotropy axes oriented along the x direction) is equivalent to the one utilized for planar anisotropy provided that, besides the substitution $\vartheta \to \varphi$, the magnetocrystalline anisotropy constant is replaced by the total anisotropy constant[33] ($K_i \to L_i = K_i - \mu_0 M_i^2/2$). However, this case will be explicitly treated in a future work.

Direct analytical solutions of the equilibrium equation exist only for its linearized form. Starting from these infinitesimal solutions, the nonlinear nucleation field equations and critical equations have been analytically deduced and then solved by utilizing standard numerical methods, with high precision and within wide ranges of the parameters, and with very low computation times. Regarding instead the finite equilibrium solutions needed to generate the complete magnetization curves, they have been calculated by means of static simulations, based on the shooting method.[43] In order to further check the validity of the obtained results, we have also performed dynamic simulations based on the integration of the Landau-Lifschitz-Gilbert (LLG) equation[44] of the bilayer with a one-dimensional grid on the x axis.[45] The boundary conditions of Sec. II A do not require to be explicitly imposed in the case of dynamic simulations since they are implicitly fulfilled, being related to the exchange coupling strength.

The results of the model can also be applied to a symmetric trilayer or to an infinite periodic soft/hard multilayer. In the case of a trilayer, one has to consider the half thickness of the intermediate layer instead of its whole thickness, while in the case of multilayers, the half thickness of both layers has to be taken into account.[33,46,47]

III. BILAYER WITH IDEAL HARD PHASE

First of all we consider the case in which the hard phase of the bilayer has an infinite anisotropy ($K_2 = \infty$) so that its magnetization is everywhere oriented along the easy direction. This approximation allows us to describe in a simplified form the general mathematical treatment leading to the expression of the nucleation field equations and of the critical equations. Moreover the phase diagram can be easily drawn as a function of the interface coupling strength.

A. Antiparallel nucleation field and phase diagram

Due to the antiferromagnetic coupling at the soft/hard interface, the magnetization process is studied starting from the equilibrium state in which the two layers are completely saturated along opposite directions (antiparallel state). In particular we consider the antiparallel state in which the hard layer has positive saturation so that the overall magnetization is $M_a = (-M_1 t_1 + M_2 t_2)/(t_1 + t_2)$. If we increment the applied field starting from this state, the magnetization curve is characterized by a nucleation field H_{n1} (also referred to in the literature[7,27,28] as the bending field) at which the magnetic moments of the soft phase start to deviate from the initial state either reversibly or irreversibly. The nucleation field turns out to be (see the Appendix) the solution $H = H_{n1}$ of the nucleation field equation

$$A_1 \gamma_1 \tan(\gamma_1 t_1) = -J_{12}, \tag{2}$$

where $\gamma_1(H) = \sqrt{\alpha_1/2 - \beta_1}$, $\alpha_1(H) = \mu_0 M_1 H/A_1$, $\beta_1 = K_1/A_1$, and $H \geqslant H_{a1} = 2K_1/(\mu_0 M_1)$. The nucleation field equation (2) has solutions for $H_{a1} \leqslant H \leqslant H_{n1,\text{strong}}$, where H_{a1} is the anisotropy field of the soft phase, and $H_{n1,\text{strong}} = H_{a1} + A_1\pi^2/(2\mu_0 M_1 t_1^2)$ is the solution in the case of strong coupling, for which Eq. (2) reduces to $\gamma_1 t_1 = \pi/2$. For decreasing $|J_{12}|$ or increasing t_1 values, the nucleation field value diminishes, thus approaching the anisotropy field H_{a1}.

The nucleation process can be reversible or irreversible, depending on the sign of the second energy variation at nucleation (see the Appendix). It is thus possible to distinguish between two different magnetization reversal regimes of the soft layer [see Fig. 1(b)]. In the exchange-spring regime (labeled as ES1) the magnetization curve shows a reversible portion that gradually starts from the nucleation point. On the contrary, in the decoupled magnet regime (labeled as DM1) the magnetization at nucleation undergoes an irreversible jump toward the parallel state, in which both soft and hard layers are saturated along the positive direction. Typically, but not necessarily, during this jump the magnetization reaches an intermediate state and then it follows a reversible path that gradually tends to approach the parallel state. Starting from the expression of second energy variation at nucleation (see the Appendix), the antiparallel critical equation

$$p_1 \left[\frac{3}{\cos^2(\gamma_1 t_1)} \left(1 + \frac{2\gamma_1 t_1}{\sin(2\gamma_1 t_1)} \right) + 2 \right] - \frac{2}{3} = 0 \tag{3}$$

can be obtained (all the reported critical equations have a positive left side when the nucleation process is reversible), where $p_1 = (\alpha_1 - 8\beta_1)/[12(\alpha_1 - 2\beta_1)]$ and γ_1 are calculated at $H = H_{n1}$. This equation, solved with respect to t_1, allows deduction of the critical thickness t_{1c} beyond which the nucleation regime changes from ES1 to DM1. In the particular case of strong coupling, the occurrence of the ES1 regime requires $t_1 < t_{1c,\text{strong}} = \pi\sqrt{A_1/(12K_1)}$. For reduced interface coupling ($|J_{12}| < \infty$), the critical thickness turns out to be $t_{1c} < t_{1c,\text{strong}}$. The critical thickness is always lower than the soft Bloch wall width d_1 ($d_i = 2\pi\sqrt{A_i/K_i}$, $i = 1,2$). Accordingly, for $t_1 > d_1$ the soft layer portion that exceeds d_1 is expected to behave as an uncoupled monolayer.

All the aspects described above can be summarized in a phase diagram by drawing in the (t_1,J_{12}) plane[28] the antiparallel critical line [see Eq. (3)] that separates the different magnetization regimes. To illustrate this phenomenology we apply the model to an example of a soft/hard system with the following typical intrinsic parameters for the soft layer: $M_1 = 1.5$ MA/m, $K_1 = 50$ kJ/m^3, $A_1 = 10^{-11}$J/m ($H_{a1} = 0.053$ MA/m, $d_1 = 89$ nm). The deduced phase diagram, reported in Fig. 2, utilizes a logarithmic vertical scale in order to show the details of the critical line for low $|J_{12}|$ values. Referring to Fig. 2 we conclude that for $|J_{12}| > \sim 0.1$ J/m^2 the critical thickness is almost coincident with that of the strong-coupling case [see the vertical asymptote drawn in Fig. 2]. The central portions of two hysteresis loops representative of both ES1 ($t_1 = 8$ nm,

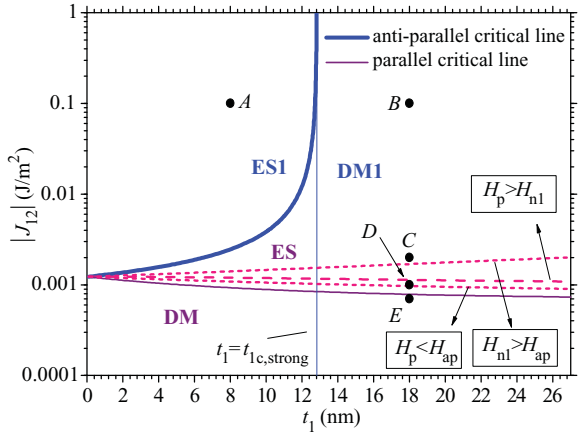

FIG. 2. (Color online) Phase diagram for the example soft/hard system with ideal hard layer. Representative points corresponding to different soft layer thicknesses are evidenced. The equifield and equienergy lines are labeled with the condition that is satisfied on the side indicated by the corresponding arrow.

$H_{n1} = 0.462$ MA/m) and DM1 ($t_1 = 18$ nm, $H_{n1} = 0.134$ MA/m) regimes for strong coupling (points A and B in Fig. 2, respectively) are reported in Fig. 3(a) assuming $M_2 = 0.7$ MA/m and $t_2 = 10$ nm. It has to be noticed that the two branches of the hysteresis loops are never connected as the ideal hard layer cannot reverse its magnetization. The DM1 loop has a small hysteresis (not appreciable in the figure) in the neighborhood of the nucleation field.[27,28] This hysteresis is due to the fact that if we reduce the applied field after the nucleation, the magnetic configuration returns to the antiparallel state by an irreversible jump at a reversal field $H_{r1} = 0.123$ MA/m $< H_{n1}$. In both loops, the magnetization never reaches the parallel state after the nucleation, due to the strong coupling that keeps the magnetic moments of the soft phase directed along the negative direction at the soft/hard interface.

B. Parallel nucleation field and phase diagram

In the presence of a reduced interface coupling, the angle between the soft and hard magnetization directions at the interface assumes finite values. Consequently, after the nucleation from the antiparallel state, the magnetization can reach the parallel state and then it can return to the initial state as well. This means that the analysis has to take into account the nucleation process from the parallel state. The corresponding parallel nucleation field $H = H_p$ is the solution of the equation

$$A_1\gamma_1 \tanh(\gamma_1 t_1) = -J_{12} \tag{4}$$

with $\gamma_1(H) = \sqrt{\alpha_1/2 + \beta_1}$ and $H \geqslant -H_{a1}$. On increasing $|J_{12}|$ from zero to the strong limit, the parallel nucleation field goes from $-H_{a1}$ to a positive infinite value. The parallel critical equation is

$$-p_1\left[\frac{3}{\cosh^2(\gamma_1 t_1)}\left(1+\frac{2\gamma_1 t_1}{\sinh(2\gamma_1 t_1)}\right)+2\right]+\frac{2}{3}=0, \tag{5}$$

where $p_1 = (\alpha_1 + 8\beta_1)[12(\alpha_1 + 2\beta_1)]$ and γ_1 are calculated at $H = H_p$.

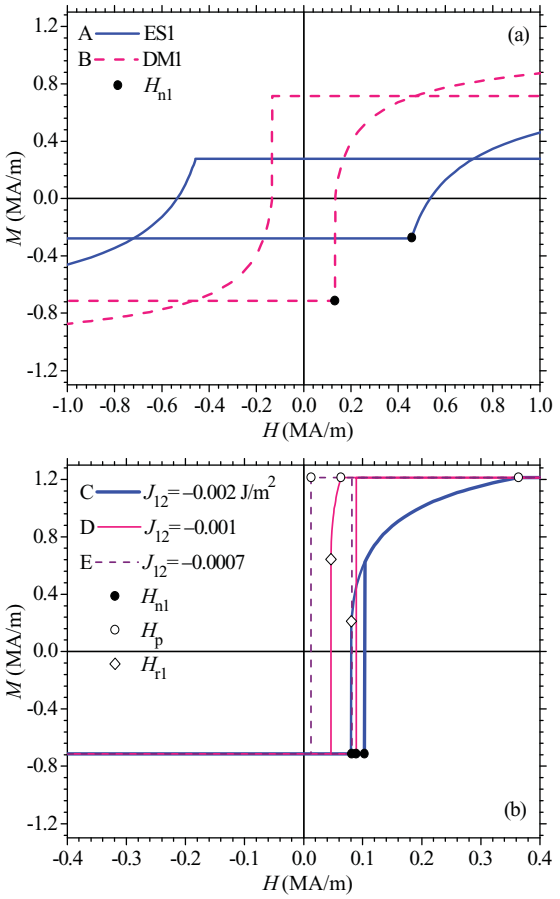

FIG. 3. (Color online) Hysteresis loops for the example soft/hard system with ideal hard layer in the case of (a) strong and (b) reduced interface coupling. The hysteresis loops correspond to points A, B, C, D, and E of the phase diagram of Fig. 2. Only the first branch of the loops is shown in (b).

In analogy to the case of Sec. III A, it is possible to draw in the (t_1, J_{12}) plane of the phase diagram the parallel critical line that separates the exchange-spring and decoupled magnet regions, which are labeled as ES and DM, respectively [see also Fig. 1(b)]. The parallel critical line for the example system is reported in Fig. 2. This line tends to the horizontal asymptote $J_{12} = -0.000\,71$ for $t_1 \cong 75$ nm $< d_1$.

The shape of the magnetization curve of a generic bilayer can be deduced starting from the antiparallel and parallel phase diagrams. This shape also depends on the comparison between H_{n1} and H_p, so that the equifield line $H_p = H_{n1}$ is introduced in the phase diagram (see Fig. 2). Considering the antiparallel nucleation process in the case $H_p > H_{n1}$, the parallel state is unstable at H_{n1} so that it cannot be reached by a direct irreversible jump. Accordingly, if we increase the applied field after the nucleation event, the magnetization approaches the parallel state by following a reversible path, since the parallel regime is of ES type in the region $H_p > H_{n1}$ of the phase diagram. As an example, a reversible saturating hysteresis loop is reported in Fig. 3(b) for the bilayer with $t_2 = 18$ nm (DM1-ES regimes) assuming $J_{12} = -0.002$ J/m^2 (point C in Fig. 2; $H_{n1} = 0.103$ MA/m, $H_p = 0.373$ MA/m). For the sake of clarity, only the first branch of the loop is shown. In this case,

the hysteresis near the nucleation field ($H_{r1} = 0.08$ MA/m) is evident in the figure.

A different behavior is observed in the region $H_p < H_{n1}$. First of all, the parallel state can be reached only in an irreversible way after nucleation from the antiparallel one; otherwise it should be $H_p > H_{n1}$. Moreover, the antiparallel regime is irreversible (DM1 regime) in this region. Then, at H_{n1} the magnetization directly jumps to the parallel state, since its energy $E_p = -\mu_0 M_1 H t_1 - \mu_0 M_2 H t_2$ is lower than the energy $E_a = \mu_0 M_1 H t_1 - \mu_0 M_2 H t_2 + 4J_{12}$ of the initial state, according to the condition $H_{n1} > H_{ap} = -2J_{12}/(\mu_0 M_1 t_1)$ (see the corresponding equienergy line drawn in Fig. 2). To illustrate this behavior, the first branches of two hysteresis loops corresponding to $J_{12} = -0.001$ J/m^2 (point D in Fig. 2; $H_{n1} = 0.089$ MA/m, $H_p = 0.063$ MA/m, $H_{ap} = 0.059$ MA/m) and $J_{12} = -0.0007$ J/m^2 (point E in Fig. 2; $H_{n1} = 0.082$ MA/m, $H_p = 0.013$ MA/m, $H_{ap} = 0.041$ MA/m) are reported in Fig. 3(b) for the bilayer with $t_1 = 18$ nm. The shapes of the two curves differ only when the applied field is reduced after the common jump to the parallel state at H_{n1}. Specifically, if one reduces the applied field below H_{n1}, the magnetization stays in the parallel state until $H = H_p$. Then, it comes back to the antiparallel state in an irreversible way; otherwise it should be $H_p > H_{n1}$. In particular, the loop related to point D (ES region) is characterized by an initial reversible path starting from the parallel state at $H = H_p$, followed by a final irreversible jump to the antiparallel state at a reversal field $H_{r1} = 0.046$ MA/m. In contrast, a direct irreversible jump from the parallel to the antiparallel state at H_p occurs if the bilayer lies in the DM region, since $H_p < H_{ap}$ according to the corresponding equienergy line reported in Fig. 2. Therefore, the hysteresis in the loop related to point E is perfectly squared and it tends to that of a true decoupled bilayer ($H_{n1} = H_{a1}$ and $H_p = -H_{a1}$) as $J_{12} \to 0$.

From the above examples, we conclude that the magnetization curve of a soft/hard ferromagnetic bilayer with antiferromagnetic interface coupling shows the occurrence of displaced hysteresis loops of the soft layer,[29] similarly to the exchange-bias phenomenology observed in ferromagnetic/antiferromagnetic structures.[48,49]

IV. GENERAL CASE

The mathematical treatment is now extended to the study of a soft/hard system with finite magnetocrystalline anisotropy of the hard layer ($K_2 < \infty$).

A. Antiparallel nucleation fields and phase diagrams

In contrast to the ferromagnetic case,[50] the magnetization curve in the presence of an antiferromagnetic interface coupling is in general characterized by two nucleation fields H_{n1} and H_{n2} from the antiparallel state. These fields can be reached by increasing and by decreasing, respectively, the initial external field value after which the magnetization begins to deviate from the antiparallel state. This departure mainly involves the soft phase for increasing fields (soft nucleation field H_{n1}) and the hard one for decreasing fields (hard nucleation field H_{n2}). Once the strength J_{12} of the interface coupling is assigned, the nucleation processes can be reversible or irreversible as a function of the thicknesses of the two layers. Therefore, the phenomenology of the magnetization process can be summarized in two magnetic phase diagrams drawn in the layer thicknesses plane (t_1,t_2).[46,50] Unlike the case of the bilayer with ideal hard phase described in Sec. III, a third regime of magnetization, the rigid magnet one, is also possible now. In this case, the nucleation process takes place through an irreversible jump of the magnetization directly to the inverted antiparallel state. A necessary condition for the rigid magnet regime to occur is that the energy $E_{-a} = -\mu_0 M_1 H t_1 + \mu_0 M_2 H t_2 + 4J_{12}$ of the inverted antiparallel state is lower than the energy E_a of the initial antiparallel one, which corresponds to the condition $M_1 t_1 > M_2 t_2$ for positive H values and $M_1 t_1 < M_2 t_2$ for negative values. These two conditions are equivalent to a negative and a positive magnetization M_a of the antiparallel state, respectively.

The nucleation field equation for the soft nucleation field $H = H_{n1}$ turns out to be

$$\frac{A_1\gamma_1 \tan(\gamma_1 t_1)}{A_2\gamma_2 \tanh(\gamma_2 t_2)} = \frac{1}{1 - \frac{A_2\gamma_2}{J_{12}} \tanh(\gamma_2 t_2)}, \tag{6}$$

where $\gamma_1(H) = \sqrt{\alpha_1/2 - \beta_1}$, $\gamma_2(H) = \sqrt{\alpha_2/2 + \beta_2}$, $\alpha_i(H) = \mu_0 M_i H/A_i$, and $\beta_i = K_i/A_i$ ($i = 1,2$). One can show that the nucleation field satisfies the condition $H_{a1} < H_{n1} < [1 + \pi^2 A_1/(4t_1^2 K_1)]H_{a1}$. When $t_2 \to \infty$, the nucleation field turns out to be independent of the hard layer thickness since $\tanh(\gamma_2 t_2) \to 1$, while for $t_2 \to 0$ it tends to the nucleation field H_{a1} of the soft monolayer. The expression for the soft antiparallel critical equation is

$$\begin{aligned} & p_1\omega_1^3 \left\{ \frac{3}{\cos^2(\gamma_1 t_1)} \left[1 + \frac{2\gamma_1 t_1}{\sin(2\gamma_1 t_1)} \right] + 2 \right\} \\ & - p_2\omega_2^3 \left\{ \frac{3}{\cosh^2(\gamma_2 t_2)} \left[1 + \frac{2t_2\gamma_2}{\sinh(2\gamma_2 t_2)} \right] + 2 \right\} \\ & - \frac{2}{3}(\omega_1 - \omega_2)^3 = 0, \end{aligned} \tag{7}$$

where $p_1(H) = (\alpha_1 - 8\beta_1)/[12(\alpha_1 - 2\beta_1)]$, $p_2(H) = (\alpha_2 + 8\beta_2)/[12(\alpha_2 + 2\beta_2)]$, $\omega_1(H) = 1/[A_1\gamma_1 \tan(\gamma_1 t_1)]$, $\omega_2(H) = 1/[A_2\gamma_2 \tanh(\gamma_2 t_2)]$, γ_1, and γ_2, are calculated at $H = H_{n1}$.

Analogously one finds that the nucleation field equation for the hard nucleation field $H = H_{n2}$ is

$$\frac{A_2\gamma_2 \tan(\gamma_2 t_2)}{A_1\gamma_1 \tanh(\gamma_1 t_1)} = \frac{1}{1 - \frac{A_1\gamma_1}{J_{12}} \tanh(\gamma_1 t_1)}, \tag{8}$$

where $\gamma_1(H) = \sqrt{-\alpha_1/2 + \beta_1}$ and $\gamma_2(H) = \sqrt{-\alpha_2/2 - \beta_2}$. The hard nucleation field satisfies the condition $-[1 + \pi^2 A_1/(4t_1^2 K_1)]H_{a2} < H_{n2} < -H_{a2}$, where $H_{a2} = 2K_2/(\mu_0 M_2)$ is the anisotropy field of the hard layer. Therefore the antiferromagnetic interface coupling implies an increase of the switching field of the hard phase too. The nucleation field turns out to be independent of the soft layer thickness when $t_1 \to \infty$ and it tends to the nucleation field $-H_{a2}$ of the hard monolayer for $t_1 \to 0$.

The hard antiparallel critical equation is

$$-\omega_1^3 p_1\left\{\frac{3}{\cosh^2(\gamma_1 t_1)}\left[1+\frac{2t_1\gamma_1}{\sinh(2\gamma_1 t_1)}\right]+2\right\} + p_2\omega_2^3\left\{\frac{3}{\cos^2(\gamma_2 t_2)}\left[1+\frac{2\gamma_2 t_2}{\sin(2\gamma_2 t_2)}\right]+2\right\} + \frac{2}{3}(\omega_1-\omega_2)^3 = 0, \quad (9)$$

where $\omega_1(H) = 1/[A_1\gamma_1 \tanh(\gamma_1 t_1)]$ and $\omega_2(H) = 1/[A_2\gamma_2 \tan(\gamma_2 t_2)]$, together with p_1, p_2, γ_1, and γ_2, are calculated at $H = H_{n2}$.

B. Strong interface coupling

The model described above is now applied to the example soft/hard system assuming a strong interface coupling ($J_{12} \to -\infty$ or equivalently $\omega_1 = \omega_2$), and setting $K_2 = 2$ MJ/m^3 and $A_2 = A_1 = 10^{-11}$ J/m ($H_{a2} = 4.55$ MA/m, $d_2 = 14$ nm). Unlike the case of ferromagnetic interface coupling, here the magnetization, once nucleated from the antiparallel state, cannot reach the parallel state due to the strong antiferromagnetic interface coupling. The calculated soft and hard phase diagrams reported in Figs. 4(a) and 4(b), respectively, show the occurrence of all three exchange-spring, decoupled magnet, and rigid magnet regimes, which are labeled as ES1, DM1, RM1 and ES2, DM2, RM2 in the soft and hard phase diagrams, respectively [see also Fig. 1(b)]. Considering first the soft phase diagram [strong case of Fig. 4(a)], the line that separates the RM1 from the DM1 region (bifurcation line) has been obtained by exploiting the fact that no finite equilibrium solution exists for systems of the RM1 region. The vertical asymptote of the critical line, which is the boundary of the DM1 region, is placed at $t_1 = 10.5$ nm ($t_1 \cong 0.1 d_1$). This asymptote is related to the fact that the hard layer portion sufficiently far from the interface behaves as an uncoupled monolayer. Analogously, the bifurcation line tends toward a horizontal asymptote given that also the soft layer portion sufficiently far from the interface, behaves as an uncoupled monolayer. The RM1 region stays on the right of the $M_1 t_1 = M_2 t_2$ line where the inverted antiparallel state has a lower energy than the noninverted one, due to the positive values of H_{n1}. Accordingly, by expanding Eqs. (6) and (7) to the first order in t_1 and t_2, one obtains that for strong coupling the antiparallel critical line approaches the $M_1 t_1 = M_2 t_2$ line near the origin of the phase diagram. The hard phase diagram, reported in Fig. 4(b), has a horizontal asymptote for the same reasons explained above. Unlike the soft phase diagram, here the RM2 region now lies on the left of the $M_1 t_1 = M_2 t_2$ line, due to the negative values of H_{n2}. As a result, the rigid magnet regimes of the two diagrams can never coexist.

In order to clearly identify the different shapes that the magnetization curve can assume, we have drawn the soft and hard phase diagrams in the same plot, which is shown in Fig 4(c). The typical hysteresis loop of an antiferromagnetically exchange-coupled soft/hard bilayer,[51] reported in Fig. 5(a), corresponds to the ES1 and DM2 nucleation regimes. In our case, the loop has been simulated for the example system assuming $t_1 = 6$ nm and $t_2 = 8$ nm [point A of Fig. 4(c); $H_{n1} = 0.46$ MA/m, $H_{n2} = -5.18$ MA/m, and

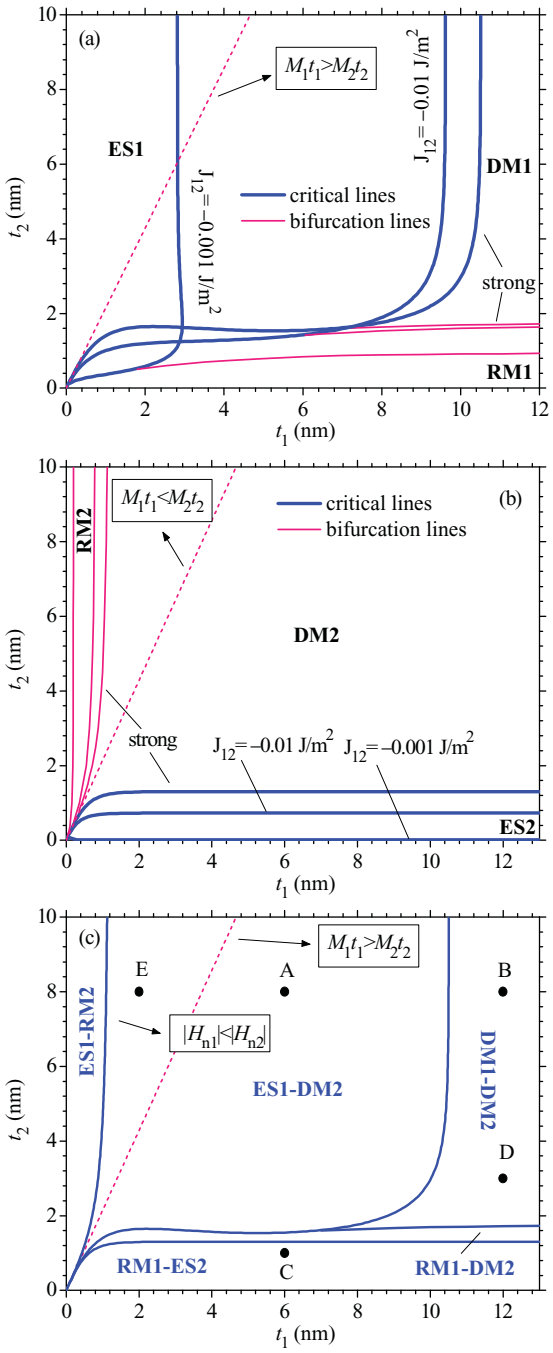

FIG. 4. (Color online) Antiparallel phase diagrams for the example soft/hard system corresponding to (a) soft nucleation process with strong and reduced interface coupling, (b) hard nucleation process with strong and reduced interface coupling, and (c) soft and hard nucleation processes with strong interface coupling. Representative points corresponding to different soft and hard layer thicknesses are evidenced in (c). The equifield and equienergy lines are labeled with the condition that is satisfied on the side indicated by the corresponding arrow.

$M_a = -0.24$ MA/m]. Accordingly, at H_{n1} the magnetization gradually starts to depart from the antiparallel state. In contrast, at $-H_{n2}$ the magnetization jumps to an intermediate state [point P of Fig. 5(a)] that, in this case, is very near to the magnetization $M_p = (M_1 t_1 + M_2 t_2)/(t_1 + t_2)$ of the parallel

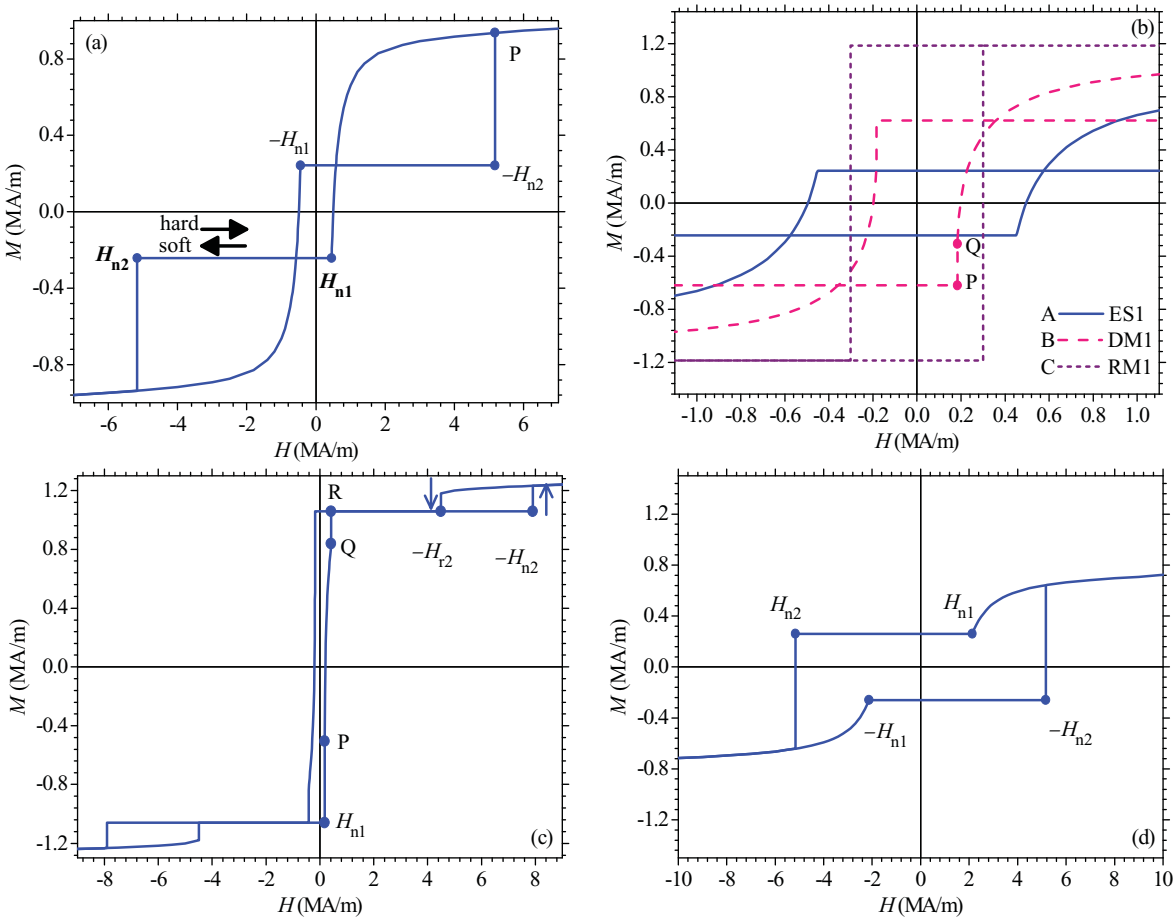

FIG. 5. (Color online) Hysteresis loops for the example soft/hard system with strong interface coupling, corresponding to the representative points of the phase diagram of Fig. 4(c): (a) point *A*, (b) points *A*, *B*, and *C*, (c) point *D*, (d) point *E*. Only the related soft parts of the loops are reported in (b).

state ($M_p = 1.04$ MA/m), as also confirmed by the corresponding magnetic configuration reported in Fig. 1(a). This jump connects the two branches of the hysteresis loop.

For comparison, the portions of the hysteresis loops related to the soft nucleation are shown in Fig. 5(b), as well as for the above-reported ES1 case, also for the additional cases of the DM1 ($t_1 = 12$ nm, $t_2 = 8$ nm, $H_{n1} = 0.18$ MA/m, $H_{n2} = -5.18$ MA/m, $M_a = -0.62$ MA/m, $M_p = 1.18$ MA/m) and RM1 ($t_1 = 6$ nm, $t_2 = 1$ nm, $H_{n1} = 0.3$ MA/m, $H_{n2} = -28$ MA/m, $M_a = -1.19$ MA/m, $M_p = 1.39$ MA/m) regimes [points *B* and *C* of Fig. 4(c), respectively]. In the DM1 case, a sudden jump of magnetization from point *P* to point *Q* takes place at H_{n1} (the small hysteresis of width 0.0012 MA/m in the neighborhood of H_{n1} is not appreciable in the figure), while the behavior at H_{n2}, not shown in the figure, is similar to that of Fig. 5(a) (DM2 regime). In the RM1 case, the reported curve portion is squared, while after the nucleation of the hard phase at H_{n2} (not shown in the figure) the curve varies reversibly with a very low susceptibility ($\chi = 0.018$, ES2 regime) tending to the inverted parallel state.

Despite the typical shape of the loop of Fig. 5(a), after the nucleation from the antiparallel state, the magnetization curve can also approach the inverted antiparallel state in both the soft and hard parts of the magnetization process. This approach can occurs in different ways depending on the comparison between the nucleation field (H_{n1} or H_{n2}) from the initial antiparallel state and the nucleation field ($-H_{n2}$ or $-H_{n1}$, respectively) related to the final inverted antiparallel state. This comparison can be suitably made by tracing the equifield line $|H_{n1}| = |H_{n2}|$ in the phase diagram of Fig. 4(c) (note that this equifield line and the hard bifurcation line are overlapped). Considering at first the soft nucleation part of the magnetization process, the magnetization can reach the inverted antiparallel state only if the bilayer lies on the right of the equienergy line $M_1 t_1 = M_2 t_2$. In this region of the phase diagram, $|H_{n1}| < |H_{n2}|$ so that the inverted antiparallel state can be reached only by a direct or final irreversible jump. As an example we report in Fig. 5(c) the simulated hysteresis loop for the case of DM1-DM2 regimes [point *D* of Fig. 4(c); $t_1 = 12$ nm, $t_2 = 3$ nm, $H_{n1} = 179$ kA/m, $H_{n2} = -7.91$ MA/m, $M_a = -1.06$ MA/m, $M_p = 1.34$ MA/m]. In the soft portion of the loop the magnetization at H_{n1} undergoes an irreversible jump to an intermediate state at point *P*, this jump being mainly due to the switching of the soft layer toward the positive magnetization direction (the jump is absent if the soft regime is of ES1 type); then, the magnetization follows a reversible path from point *P* to point *Q*, and finally it goes through a second irreversible jump from point *Q* to point *R*, at which the inverted antiparallel

state is reached (the small hysteresis of width 0.002 MA/m in the neighborhood of H_{n1} cannot be appreciated in the figure). The second jump is mainly due to the switching of the hard phase toward the negative magnetization direction. Subsequently, if we further increase the applied field H, at $H = -H_{n2}$ the magnetization of the hard layer undergoes another irreversible jump, this time toward the positive magnetization direction, and then, if we decrease the applied field, it irreversibly comes back to the antiparallel state at a reversal field $-H_{r2} < -H_{n2}$.

In the case of the hard nucleation part of the magnetization curve, the magnetization can reach the inverted antiparallel state only if the bilayer lies on the left of the equienergy line of the phase diagram. We note that in this region $M_a > 0$ and consequently $t_1 < t_2$. To illustrate this behavior, the magnetization curve obtained in particular when $|H_{n2}| > |H_{n1}|$ (right side of the equifield line) is reported in Fig. 5(d) for an example bilayer that lies in the ES1-DM2 region on the left of the equienergy line [point E of Fig. 4(c); $t_1 = 2$ nm, $t_2 = 8$ nm, $H_{n1} = 2.13$ MA/m, $H_{n2} = -5.16$ MA/m, $M_a = 0.26$ MA/m, $M_p = 0.86$ MA/m]. In this case, the magnetization can indirectly reach the inverted antiparallel state by an initial jump to the reversible path (ES1 regime) that originates from $-H_{n1}$ in the second branch of the hysteresis loop. We remark that this reversible path tends to the inverted parallel state on further decrease of the applied field value toward $-\infty$. On the contrary, the magnetization reaches the inverted antiparallel state along this path if we increase the applied field until its value becomes $-H_{n1}$. Experimental realizations showing a similar behavior in the case of asymmetric hard/soft/hard trilayers can be found, for example, in Ref. 52.

C. Reduced interface coupling

We now take into account the occurrence of a reduced coupling at the soft/hard interface. In this case, the magnetization process approaches that of a true decoupled system, characterized by a rigid behavior of both layers. In fact, the DM1 region of the soft nucleation phase diagram grows at the expense of the ES1 and RM1 portions as reported in Fig. 4(a), where the diagrams obtained for $J_{12} = -0.01$ J/m^2 and $J_{12} = -0.001$ J/m^2 are compared with that of the strong case ($J_{12} > \sim -0.1$ J/m^2). A similar trend is observed in the hard nucleation phase diagram of Fig. 4(b). In both diagrams, the asymptotes approach the graph axes and so the corresponding asymptotic thicknesses decrease with respect to the strong case. Due to the reduced interface coupling, the parallel states become accessible to the soft and hard parts of the magnetization process. As in Sec. III, the analysis therefore takes into account the nucleation process from the parallel state. We consider only the positive parallel state given that the nucleation field for the negative parallel state has the same absolute value and opposite sign. The parallel nucleation field is the solution $H = H_p$ of the parallel nucleation field equation

$$\frac{A_1\gamma_1\tanh(\gamma_1 t_1)}{A_2\gamma_2\tanh(\gamma_2 t_2)} = -\frac{1}{1+\frac{A_2\gamma_2\tanh(\gamma_2 t_2)}{J_{12}}} \tag{10}$$

with $\gamma_i(H) = \sqrt{\alpha_i/2+\beta_i}$ and $H > -H_{a1}$. In the strong-limit case ($J_{12} \to -\infty$) the parallel nucleation field can be approximated by the expression $H_p \cong 2J_{12}^2(\sqrt{A_1M_1}+\sqrt{A_2M_2})^2/(\mu_0 A_1M_1A_2M_2)$, evidencing that $H_p \to +\infty$ in this limit.

The parallel critical equation is

$$\begin{aligned} &-p_1\omega_1^3\left\{\frac{3}{\cosh^2(\gamma_1 t_1)}\left[1+\frac{2\gamma_1 t_1}{\sinh(2\gamma_1 t_1)}\right]+2\right\} \\ &-p_2\omega_2^3\left\{\frac{3}{\cosh^2(\gamma_2 t_2)}\left[1+\frac{2\gamma_2 t_2}{\sinh(2\gamma_2 t_2)}\right]+2\right\} \\ &+\frac{2}{3}(\omega_1+\omega_2)^3 = 0, \end{aligned} \tag{11}$$

where $p_i(H) = (\alpha_i + 8\beta_i)/[12(\alpha_i + 2\beta_i)]$, $\omega_i(H) = 1/[A_i\gamma_i\tanh(\gamma_i t_i)]$, and γ_i $(i = 1,2)$, are calculated at $H = H_p$. Equation (11) allows the parallel nucleation phase diagram to be deduced by drawing the related critical line. The occurrence of the hyperbolic functions in both soft and hard parts of this expression implies that both horizontal and vertical asymptotes can appear. Regarding the rigid magnet regime, a necessary condition for jumping from the parallel to the inverted parallel state is $H_p < 0$, which assure a final energy lower than the initial one. In agreement with the analysis reported in Ref. 9, the rigid magnet region, when present, does not correspond to an area of the phase diagram, but instead it is limited to a line, as also described with more particulars in the following. Therefore, this regime has a pure theoretical meaning, all the more so because the magnetization, once the parallel states are reached, can only switch between them.

The deduced parallel critical line of the example system is shown in Fig. 6 for different $|J_{12}|$ values, the exchange-spring, decoupled magnet, and rigid magnet regions being labeled as ES, DM, and RM, respectively [see also Fig. 1(b)]. For sufficiently low values of $|J_{12}|$ the magnetization regime is of DM type almost everywhere, and the behavior of the bilayer is similar to that of a true decoupled system. If we increase $|J_{12}|$, two initially joined DM regions appear in the phase diagram [see Fig. 6(a)]. Subsequently, these two regions separate and then tend to depart one from the other [see Fig. 6(b)]. In the superior DM region, which is initially bounded by a vertical and a horizontal asymptote [see Fig. 6(b)], a second vertical asymptote [see Fig. 6(c)] appears on the right of the first one at $t_1 \cong 320$ nm ($t_1 \cong 3.6\times d_1$) for $|J_{12}| = 0.0005$ J/m^2. After that, this region disappears [see Fig. 6(d)]. The inferior DM region shows two horizontal asymptotes, one of them being so close to the t_1 axis that it becomes visible only if $|J_{12}|$ is sufficiently large [see Fig. 6(d)]. Finally, for $|J_{12}| \cong 0.00176$ J/m^2 also this region collapses and the magnetization regime becomes of ES type everywhere. As regards the occurrence of two DM regions in the parallel phase diagram, in the superior DM region it is the soft layer that drives the switching of the magnetization toward the antiparallel state [see Fig. 1(b)]. In contrast, in the inferior DM region this action is performed by the hard layer, which instead tries to lead the magnetization to the inverted antiparallel state [see Fig. 1(b)], or equivalently from the inverted parallel state at $-H_p$ to the antiparallel one (see, for example, the hysteresis loop described at the end of this section). According to Ref. 9, the rigid magnet regime is present only when the superior and inferior DM regions are joined together and it corresponds to the points

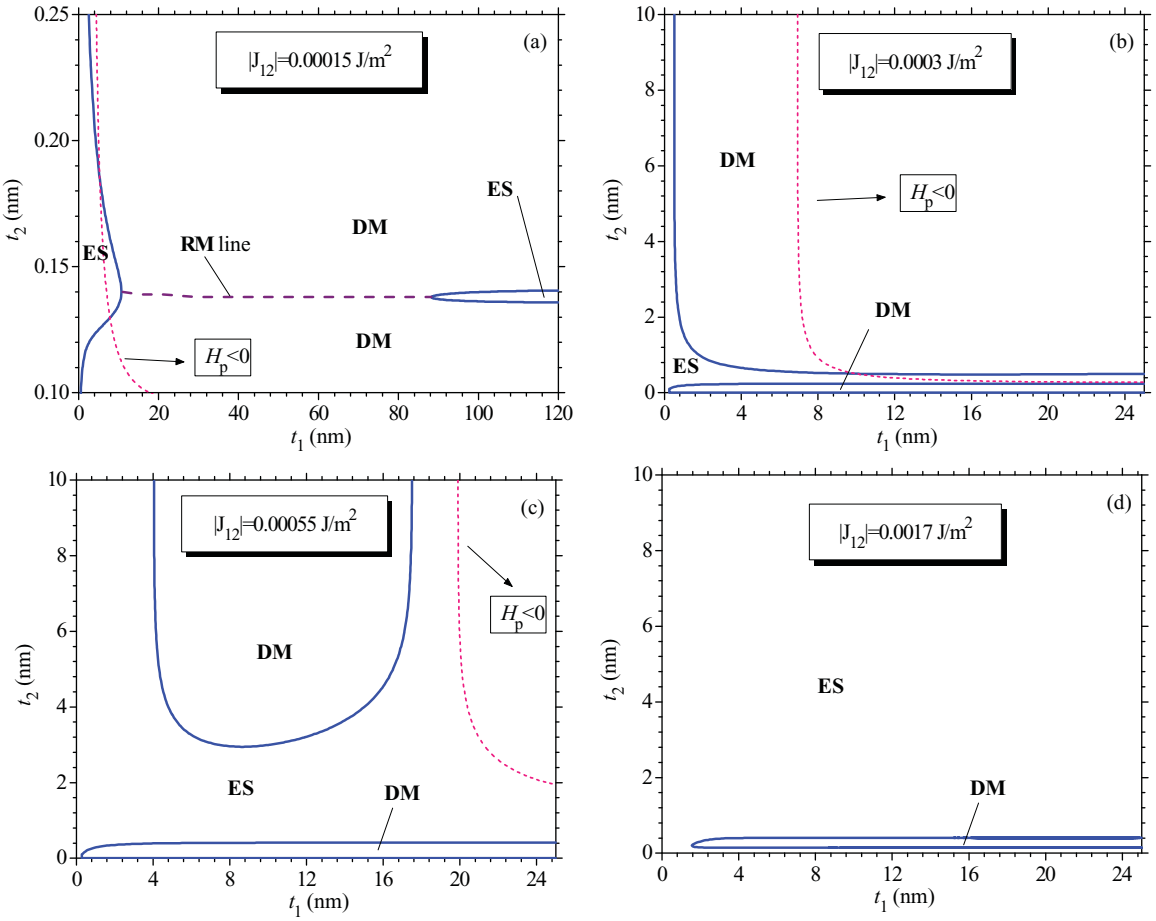

FIG. 6. (Color online) Parallel nucleation phase diagrams for the example soft/hard system corresponding to different values of the interface coupling strength. The isofield lines $H_p = 0$ are labeled with the condition that is satisfied on the side indicated by the corresponding arrow.

of the line that separates the two typical behaviors related to these regions. In fact, it is only at these limit points that both layers reverse their magnetic state and finally jump to the inverted parallel configuration. As a consequence of this behavior, the rigid magnet line can be calculated with a good approximation by seeking for the points of maximum susceptibility as a function of the hard layer thickness, since a variation of its very low value appreciably influences the character of the switching. The result ($t_2 \cong$ const $=$ 0.138 nm) is in good agreement with that ($t_2 \cong$ const $=$ 0.151 nm) obtained by applying the corresponding critical condition of Ref. 9, which is valid for the limit case of coherent rotation (this approximation can be accepted here, due to the considered low $|J_{12}|$ value). As a further remark concerning the nucleation from the parallel state, we observe that the hard and soft thicknesses beyond which this process is no longer affected by the sizes of the layers appreciably exceed the related Boch wall widths, as evidenced by the position of the asymptotes in the diagrams.

In the phase diagrams of Fig. 6 is also reported the isofield line $H_p = 0$ that identifies the region $H_p < 0$, in which the parallel state is stable in absence of the external field [in the case of Fig. 6(d), this line is outside the figure]. Moreover, only inside this region can the rigid magnet regime occur, as previously observed.

The shape of the magnetization curve of a generic bilayer can be deduced starting from the related phase diagrams, also supported by suitably defined isofield, equifield, and equienergy lines. Due to the complexity of a general analysis of the phase diagrams, we limit the application of the model to the example system for the particular case of $J_{12} = -0.0007$ J/m^2. The corresponding soft antiparallel and parallel critical lines are reported in Fig. 7 while for the clarity of the figure, the equienergy lines, whose meaning is analogous to that of Fig. 2, are not shown. Due to the low $|J_{12}|$ value, the hard nucleation regime is of DM2 type almost everywhere, since the ES2 and the RM2 regions are very close to the soft ($t_2 < 0.1$ nm) and to the hard ($t_1 < 0.15$ nm) thickness axes of the diagram, respectively. In particular it is $|H_{n2}| > |H_{n1}|$ almost everywhere. Analogously, the equifield line $H_{n2} = -H_p$ is almost coincident with the vertical axis ($t_1 < 0.18$) so that we can assume $H_{n2} < -H_p$.

The magnetization curves of bilayers whose representative points lie inside the region $H_p > H_{n1}$ but outside the RM1 region of the phase diagram (see points *A* and *B* of Fig. 7), reach the parallel state in a reversible way after the soft nucleation at H_{n1}. This path can be completely reversible (point *A* of Fig. 7,

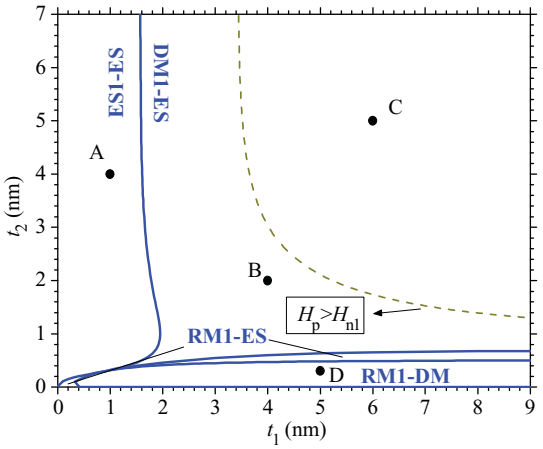

FIG. 7. (Color online) Overlapped soft antiparallel and parallel nucleation phase diagrams for the example soft/hard system corresponding to $J_{12} = -0.0007$ J/m^2. Representative points corresponding to different soft and hard layer thicknesses are evidenced. The equifield line is labeled with the condition that is satisfied on the side indicated by the corresponding arrow.

regime ES1) as happens in the strong case. It can also start with an irreversible jump to an intermediate state (point *B* of Fig. 7, regime DM1) similarly to the curve *C* of Fig. 3(b). The hard nucleation part of the magnetization curve is instead similar to that related to point *C* of Fig. 7 (see below).

We now consider a point of the phase diagram (point *C* in Fig. 7; $t_1 = 6$ nm, $t_2 = 5$ nm, $H_{n1} = 0.15$ MA/m, $H_{n2} = -4.81$ MA/m, $H_p = 0.12$ MA/m, $M_a = -0.5$ MA/m, $M_p = 1.14$ MA/m) inside the region $H_p < H_{n1}$ and again outside the RM1 region. The corresponding soft nucleation part of the magnetization process is similar to the second curve (curve *D*) of Fig. 3(b). In analogy to what happens in the soft part of the magnetization process, in the case of the hard part the magnetization directly jumps to the inverted parallel state at H_{n2} [see Fig. 8(a)]. After that, if we reduce $|H|$ the magnetization stays in this state until $H = -H_p$ and then, exactly as in the soft part of the second branch of the hysteresis loop, it reaches the inverted antiparallel state by following an initial reversible path (not appreciable in the figure) and by doing a final irreversible jump at a reversal field $H_{r2} = -H_{r1} \cong -H_p$.

If we finally consider the points of the phase diagram lying in the RM1 region, the magnetization at H_{n1} goes to the inverted antiparallel state rather than to the parallel one, which is not stable since $H_{n1} < H_p$. Therefore, the parallel states are accessed only in the hard parts of the magnetization curve. In fact, at H_{n2} the magnetization jumps (DM2 regime) to the inverted parallel state, since this state is stable ($H_{n2} < -H_p$) and since the energy $E_{-p} = \mu_0 M_1 H t_1 + \mu_0 M_2 H t_2$ of the inverted parallel state is lower than initial energy E_a, according to the condition $H_{n2} < -H_{-ap} = 2J_{12}/(\mu_0 M_2 t_2)$ (the corresponding equienergy line is almost coincident with the vertical axis of the phase diagram, so that $H_{n2} < -H_{-ap}$ almost everywhere). The magnetization comes back to the antiparallel state at $-H_p$, through a possibly initially reversible path (regime RM1-ES) and a final or direct irreversible jump (regimes RM1-ES and RM1-DM, respectively). An example

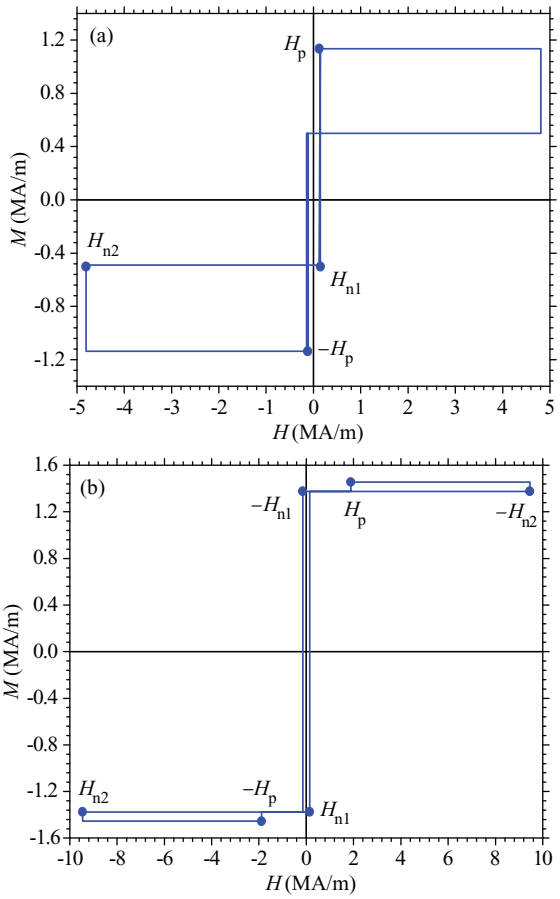

FIG. 8. (Color online) Hysteresis loops for the example soft/hard system corresponding to (a) point *C* and (b) point *D* of the phase diagram of Fig. 7.

of such a loop is reported in Fig. 8(b) for the bilayer corresponding to point *D* of Fig. 7 (regime RM1-DM; $t_1 = 5$ nm, $t_2 = 0.3$ nm, $H_{n1} = 0.12$ MA/m, $H_{n2} = -9.46$ MA/m, $H_p = 1.89$ MA/m, $M_a = -1.38$ MA/m, $M_p = 1.45$ MA/m). We note in particular that the jump from the inverted parallel to the antiparallel state at $-H_p$ on the first branch of the hysteresis loop, or equivalently the jump from the parallel to the inverted antiparallel state at H_p on the second branch of the hysteresis loop, is typical of the bilayers belonging to the inferior DM region of the parallel phase diagrams.

V. CONCLUSIONS

A general continuum micromagnetic modeling of the interlayer and intralayer exchange interaction has been presented and the general boundary conditions at the interface between two ferromagnetic phases have been derived. Then the continuum micromagnetic theory has been applied to perfect soft/hard bilayers with uniaxial anisotropy and antiferromagnetic interface coupling in order to analyze the corresponding magnetization process, which is characterized by a nonuniform rotation of magnetization inside the two phases. The essential aspects of the mathematical procedure have been described for the particular case of an ideal hard phase with infinite anisotropy. In the general case we have shown that when the external field is applied along the easy direction, which is

identical in the two layers, the magnetization can leave the saturated antiparallel state at two different nucleation fields, each mainly concerning only one of the two ferromagnetic phases. Moreover, the saturated parallel state can also be accessed in the presence of an interface coupling that is reduced with respect to the strong case. Therefore, the description of the magnetization process requires that the nucleation from the parallel state is taken into account, so that three different parts related to the antiparallel soft nucleation, the antiparallel hard nucleation, and the parallel nucleation appear in the magnetization curves. Different magnetization regimes, which depend on the reversible or irreversible character of the various nucleation events, can be identified by solving the corresponding critical equations. Accordingly, the behavior of the possible bilayers can be summarized in suitable phase diagrams as a function of intrinsic and extrinsic parameters. The nucleation field equations and the critical equations have been analytically deduced and then applied to a typical soft/hard system with planar anisotropy. The corresponding phase diagrams have been calculated as a function of the layer thicknesses and of the interface coupling strength, obtaining a rich variety of possible behaviors. Additional equations, related to the comparison between the different nucleation fields and to the comparison between the energies of different antiparallel and parallel saturated states, have also been utilized to include additional information in the phase diagrams. Static and dynamic simulations of hysteresis loops have been performed to support the analysis based on the phase diagrams. All the results obtained with the simulations have turned out to be in perfect mutual agreement. As a secondary result, we have found that the influence of the interface coupling in the parallel nucleation process extends inside the two ferromagnetic phases at distances appreciably larger than the corresponding Bloch wall widths. Finally, we observe that all the deduced equations have been accurately tested with the aim of making them available for possible applications to systems characterized by whatever parameter values and also by perpendicular anisotropy.

ACKNOWLEDGMENTS

This work was supported by the Italian Ministry of University and Research through PRIN2008 Project entitled "Thermal stability of exchange-spring planar magnetic nanostructures with perpendicular and lateral exchange coupling (20084LFC29)."

APPENDIX

The equilibrium equation $\vec{m} \times \vec{H}_{\text{eff}} = 0$ inside the considered soft/hard bilayers assumes the form

$$\frac{d^2\vartheta}{dx^2} - \frac{K_i}{A_i}\sin\vartheta\cos\vartheta - \frac{\mu_0 M_i}{2A_i}H\sin\vartheta = 0 \tag{A1}$$

with boundary conditions

$$\left.\frac{d\vartheta}{dx}\right|_{x_1} = 0, \quad A_1\left.\frac{d\vartheta}{dx}\right|_{x_{0^-}} = A_2\left.\frac{d\vartheta}{dx}\right|_{x_{0^+}} = J_{12}\sin(\vartheta_{0^+} - \vartheta_{0^-}), \quad \left.\frac{d\vartheta}{dx}\right|_{x_2} = 0. \tag{A2}$$

In the ideal case in which the hard phase has an infinite anisotropy ($K_2 = \infty$), the equilibrium equation (A1) inside the soft layer ($i = 1$) becomes

$$\frac{d^2\psi}{dx^2} + \left(\mu_0\frac{M_1}{2A_1}H - \frac{K_1}{A_1}\cos\psi\right)\sin\psi = 0, \tag{A3}$$

where we have introduced the angle $\psi = \pi - \vartheta$. The corresponding boundary conditions (A2) turn into

$$\left.\frac{d\psi}{dx}\right|_{x_1} = 0, \quad A_1\left.\frac{d\psi}{dx}\right|_{x_{0^-}} = J_{12}\sin\psi_{0^-}. \tag{A4}$$

In the strong-coupling limit ($J_{12}\to-\infty$) the second boundary condition simplifies to $\psi_{0^-} = 0$. Equations (A3) and (A4) can also be deduced by minimizing the energy per unit area of the soft layer:

$$E = \int_{x_1}^{x_0}\left[A_1\left(\frac{d\psi}{dx}\right)^2 + \mu_0 M_1 H\cos\psi + K_1\sin^2\psi\right]dx + 2J_{12}(1+\cos\psi_{0^-}). \tag{A5}$$

We now consider an infinitesimal solution $\psi + \eta$ (ψ and η being the first- and third-order contributions, respectively) of Eq. (A3) in the neighborhood of the antiparallel state $\psi = 0$ and in the neighborhood h of the nucleation field H. Then, from Eq. (A3) we obtain the equation for the first-order contribution

$$\frac{d^2\psi}{dx^2} + \left(\mu_0\frac{M_1}{2A_1}H - \frac{K_1}{A_1}\right)\psi = 0, \tag{A6}$$

with boundary conditions

$$\left.\frac{d\psi}{dx}\right|_{x_1} = 0, \quad A_1\left.\frac{d\psi}{dx}\right|_{x_{0^-}} = J_{12}\psi_{0^-}, \tag{A7}$$

and the equation for the third-order contribution

$$\frac{d^2\eta}{dx^2} + \left(\mu_0\frac{M_1}{2A_1}H - \frac{K_1}{A_1}\right)\eta = -\mu_0\frac{M_1}{2A_1}h\psi - \frac{1}{12}(8\beta_1 - \alpha_1)\psi^3 \tag{A8}$$

with boundary conditions

$$\left.\frac{d\eta}{dx}\right|_{x_1} = 0, \quad A_1\left.\frac{d\eta}{dx}\right|_{x_{0^-}} = J_{12}\left(\eta_{0^-} - \frac{\psi_{0^-}^3}{6}\right). \tag{A9}$$

We note that the function ψ in Eq. (A8) is the first-order contribution, solution of Eq. (A6). This solution ψ exists if and only if H fulfills the nucleation field equation (2) and it takes the form

$$\psi(x) = \frac{\psi_{0^-}}{\cos(\gamma_1 t_1)}\cos[\gamma_1(x - x_1)]. \tag{A10}$$

Analogously, the third-order contribution η, solution of Eq. (A8) (which can be obtained by using the method of variation of parameters[53]), exists if and only if the following relation between the first-order infinitesimal constant ψ_{0^-} and

the infinitesimal field increment h is satisfied:

$$\psi_{0^-}^2 = \frac{\mu_0 \frac{M_1}{A_1}\left(\frac{1}{\gamma_1^2} + \frac{2t_1}{\gamma_1 \sin(2\gamma_1 t_1)}\right)}{p_1\left[\frac{3}{\cos^2(\gamma_1 t_1)}\left(1 + \frac{2\gamma_1 t_1}{\sin(2\gamma_1 t_1)}\right) + 2\right] - \frac{2}{3}} h. \quad \text{(A11)}$$

If one calculates the variation of the energy at nucleation with respect to the antiparallel state, then the first energy variation, which is obtained by considering the second-order terms in Eq. (A5), is obviously vanishing. On the contrary, the second energy variation at nucleation, which is obtained by considering the fourth-order terms[54,55] in Eq. (A5) and by utilizing Eqs. (2), (A8), (A9), (A10), and (A11), turns out to be

$$\Delta E = -\frac{1}{8\omega_1}\left\{p_1\left[\frac{3}{\cos^2(\gamma_1 t_1)}\left(1+\frac{2\gamma_1 t_1}{\sin(2\gamma_1 t_1)}\right)+2\right]-\frac{2}{3}\right\}\psi_{0^-}^4. \quad \text{(A12)}$$

Therefore, if

$$p_1\left[\frac{3}{\cos^2(\gamma_1 t_1)}\left(1 + \frac{2\gamma_1 t_1}{\sin(2\gamma_1 t_1)}\right) + 2\right] - \frac{2}{3} > 0, \quad \text{(A13)}$$

the nucleated state has an energy lower than that of the antiparallel state at the same field $H + h$. In the opposite case the nucleated *equilibrium* state has a greater energy, thus representing for the antiparallel state an energy barrier that vanishes at the nucleation field H. These conclusions are in agreement with the stability criterion[50] based on the sign of the susceptibility χ at the nucleation field, since

$$\chi = -\mu_0 M_1^2 \left(\frac{t_1}{\cos^2(\gamma_1 t_1)} + \frac{\tan(\gamma_1 t_1)}{\gamma_1}\right)^2 \frac{\psi_{0^-}^4}{32(t_1 + t_2)\Delta E}. \quad \text{(A14)}$$

[1] R. H. Victora and X. Shen, IEEE Trans. Magn. **41**, 537 (2005).
[2] E. E. Fullerton, J. S. Jiang, and S. D. Bader, J. Magn. Magn. Mater. **200**, 392 (1999).
[3] E. E. Fullerton, J. S. Jiang, M. Grimsditch, C. H. Sowers, and S. D. Bader, Phys. Rev. B **58**, 12193 (1998).
[4] F. Montaigne, S. Mangin, and Y. Henry, Phys. Rev. B **67**, 144412 (2003).
[5] K. Mibu, T. Nagahama, and T. Shinjo, J. Magn. Magn. Mater. **163**, 75 (1996).
[6] E. F. Kneller and R. Hawig, IEEE Trans. Magn. **27**, 3588 (1991).
[7] E. Goto, N. Hayashi, T. Miyashita, and K. Nakagawa, J. Appl. Phys. **36**, 2951 (1965).
[8] H. J. Richter, J. Phys. D **40**, R149 (2007).
[9] G. H. Guo, G. F. Zhang, L. Y. Sun, and P. A. J. de Groot, Chin. Phys. Lett. **25**, 2634 (2008).
[10] E. E. Fullerton, D. T. Margulies, M. E. Schabes, M. Carey, B. Gurney, A. Moser, M. Best, G. Zeltzer, K. Rubin, H. Rosen, and M. Doerner, Appl. Phys. Lett. **77**, 3806 (2000).
[11] B. R. Acharya, J. N. Zhou, M. Zheng, G. Choe, E. N. Abarra, and K. E. Johnson, IEEE Trans. Magn. **40**, 2383 (2004).
[12] S. N. Piramanayagam, J. Appl. Phys. **102**, 011301 (2007).
[13] S. N. Piramanayagam, K. O. Aung, S. Deng, and R. Sbiaa, J. Appl. Phys. **105**, 07C11 (2009).
[14] J. M. L. Beaujour, S. N. Gordeev, G. J. Bowden, P. A. J. de Groot, B. D. Rainford, R. C. C. Ward, and M. R. Wells, Appl. Phys. Lett. **78**, 964 (2001).
[15] T. Hauet, F. Montaigne, M. Hehn, Y. Henry, and S. Mangin, Phys. Rev. B **79**, 224435 (2009).
[16] D. V. Dimitrov, J. van Ek, Y. F. Li, and J. Q. Xiao, J. Appl. Phys. **87**, 6427 (2000).
[17] R. C. Sousa, Z. Zhang, and P. P. Freitas, J. Appl. Phys. **91**, 7700 (2002).
[18] X. G. Xu, D. L. Zhang, X. Q. Li, J. Bao, Y. Jiang, and M. B. A. Jali, J. Appl. Phys. **106**, 123902 (2009).
[19] M. Sawicki, G. J. Bowden, P. A. J. de Groot, B. D. Rainford, J. M. L. Beaujour, R. C. C. Ward, and M. R. Wells, Phys. Rev. B **62**, 5817 (2000).
[20] N. Persat, H. A. M. van den Berg, and A. Dinia, Phys. Rev. B **62**, 3917 (2000).
[21] J. F. Bobo, H. Kikuchi, O. Redon, E. Snoeck, M. Piecuch, and R. L. White, Phys. Rev. B **60**, 4131 (1999).
[22] M. Buchmeier, B. K. Kuanr, R. R. Gareev, D. E. Bürgler, and P. Grünberg, Phys. Rev. B **67**, 184404 (2003).
[23] W. F. Brown Jr., *Micromagnetics* (Wiley Interscience, New York, 1963).
[24] K. Yu. Guslienko, O. Chubykalo-Fesenko, O. Mryasov, R. Chantrell, and D. Weller, Phys. Rev. B **70**, 104405 (2004).
[25] A. Bill and H.B. Braun, J. Magn. Magn. Mater. **272**, 1266 (2004).
[26] S. Mangin, F. Montaigne, and A. Schuhl, Phys. Rev. B **68**, 140404(R) (2003).
[27] G. J. Bowden, K. N. Martin, B. D. Rainford, and P. A. J. de Groot, J. Phys. Condens. Matter **20**, 015209 (2008).
[28] G. H. Guo, G. F. Zhang, and X. G. Wang, J. Appl. Phys. **108**, 043919 (2010).
[29] S. Mangin, L. Thomas, F. Montaigne, W. Lin, T. Hauet, and Y. Henry, Phys. Rev. B **80**, 224424 (2009).
[30] B. Dieny, J. P. Gavigan, and J. P. Rebouillat, J. Phys. Condens. Matter **2**, 159 (1990).
[31] D. C. Worledge, Appl. Phys. Lett. **84**, 2847 (2004).
[32] A. Layadi, J. Appl. Phys. **100**, 083904 (2006).
[33] G. Asti, M. Ghidini, R. Pellicelli, C. Pernechele, M. Solzi, F. Albertini, F. Casoli, S. Fabbrici, and L. Pareti, Phys. Rev. B **73**, 094406 (2006).
[34] O. Hellwig, A. Berger, J. B. Kortright, and E. E. Fullerton, J. Magn. Magn. Mater. **319**, 13 (2007).
[35] N. S. Kiselev, C. Bran, U. Wolff, L. Schultz, A. N. Bogdanov, O. Hellwig, V. Neu, and U. K. Rößler, Phys. Rev. B **81**, 054409 (2010).
[36] G. M. Choi, I. J. Shin, B. C. Min, and K. H. Shin, J. Appl. Phys. **108**, 073913 (2010).
[37] Z. Y. Liu, F. Zhang, H. L. Chen, B. Xu, D. L. Yu, J. L. He, and Y. J. Tian, Phys. Rev. B **79**, 024427 (2009).
[38] P. Grünberg, R. Schreiber, Y. Pang, M. B. Brodsky, and H. Sowers, Phys. Rev. Lett. **57**, 2442 (1986).

[39]T. Klein, R. Röhlsberger, O. Crisan, K. Schlage, and E. Burkel, Thin Solid Films **515**, 2531 (2006).
[40]D. E. Bürgler, D. M. Schaller, C. M. Schmidt, F. Meisinger, J. Kroha, J. McCord, A. Hubert, and H. J. Güntherodt, Phys. Rev. Lett. **80**, 4983 (1998).
[41]J. Fidler and T. Schrefl, J. Phys. D **33**, R135 (2000).
[42]T. Leineweber and H. Kronmüller, J. Magn. Magn. Mater. **176**, 145 (2004).
[43]W. H. Press, S. A. Teukolsky, W. T. Vetterling, and B. P. Flannery, *Numerical Recipes: The Art of Scientific Computing,* 3rd ed. (Cambridge University Press, Cambridge, 2007), Chap. 18.
[44]D. Suess, V. Tsiantos, T. Schrefl, J. Fidler, W. Scholz, H. Forster, R. Dittrich, and J. J. Miles, J. Magn. Magn. Mater. **248**, 298 (2002).
[45]M. Grimsditch, R. Camley, E. E. Fullerton, S. Jiang, S. D. Bader, and C. H. Sowers, J. Appl. Phys. **85**, 5901 (1999).
[46]M. Ghidini, G. Asti, R. Pellicelli, C. Pernechele, and M. Solzi, J. Magn. Magn. Mater. **316**, 159 (2007).
[47]R. Pellicelli, M. Solzi, V. Neu, K. Häfner, C. Pernechele, and M. Ghidini, Phys. Rev. B **81**, 184430 (2010).
[48]W. H. Meiklejohn and C. P. Bean, Phys. Rev. **105**, 904 (1957).
[49]J. Nogués and I. K. Schuller, J. Magn. Magn. Mater. **192**, 203 (1999).
[50]G. Asti, M. Solzi, M. Ghidini, and F. M. Neri, Phys. Rev. B **69**, 174401 (2004).
[51]G. J. Bowden, J. M. L. Beaujour, A. A. Zhukov, B. D. Rainford, P. A. J. de Groot, R. C. C. Ward, and M. R. Wells, J. Appl. Phys. **93**, 6480 (2003).
[52]S. Wüchner, J. C. Toussaint, and J. Voiron, Phys. Rev. B **55**, 11576 (1997).
[53]W. E. Boyce and R. C. DiPrima, *Elementary Differential Equations and Boundary Value Problems* (Wiley Interscience, New York, 1965).
[54]A. Aharoni, J. Appl. Phys. **30**, 70S (1959).
[55]G. P. Zhao and X. L. Wang, Phys. Rev. B **74**, 012409 (2006).